Waves and Vortices Driven by Interfacial Fluxes

Lecturer: Kerry A. Emanuel
Notes written by: Malte F. Jansen & Yutian Wu

November 17, 2008

Figure 1: Satellite image of Hurricane Floyd approaching the east coast of Florida in 1999. The image has been digitally enhanced to lend a three-dimensional perspective. Credit: NASA/Goddard Space Flight Center.

1 Atmospheric Boundary Layers

The flux of sensible and latent heat at the surface boundary layer can drive major atmospheric disturbances as for example hurricanes. On the other hand the surface winds associated with these disturbances, influence the surface fluxes which leads to an essential feedback. Our understanding of boundary layer fluxes is therefore crucial for the understanding of many meteorological phenomena. We will here derive some simple scaling laws for the simplified cases of a boundary below a semi-infinite domain. First we will consider the cases of convective and mechanically driven turbulence separately and then briefly discuss how the results might be generalized. In section 1.4 we will show how the interaction between surface winds and surface heat flux can lead to growing wave-like perturbations.

Finally section 1.5 will show that turbulent heat flux in the boundary layer is essential to wipe out the thermodynamically unstable radiative equilibrium state.

1.1 Convective Boundary Layers

Assume a lower boundary under a semi-infinite domain. The turbulent flux of buoyancy through the boundary at z=0 is then given by

$$Q = \overline{w'B'} = -\int_0^\infty \dot{B} dz \,, \tag{1}$$

where $\dot{B}$ denotes the radiative cooling in the domain. The buoyancy flux has the dimension of a length squared over a time cubed:

$$Q \sim L^2 t^{-3} \tag{2}$$

Since no length scale is intrinsic to the system, dimensional analysis gives a velocity scale

$$w' \sim (Qz)^{\frac{1}{3}} \tag{3}$$

i.e. the turbulent velocity increases as $z^{\frac{1}{3}}$. Similarly we find

$$B' \sim Q^{\frac{2}{3}} z^{-\frac{1}{3}} \tag{4}$$

This would imply infinite buoyancy perturbations as $z \to 0$. To overcome this problem we have to consider a thin surface layer in which diffusion or the roughness of the boundary becomes important. For atmospheric applications the boundary roughness scale is generally much larger than the scale at which molecular diffusion starts to play a role. The above scaling laws then apply only down to the height of the boundary layer roughness scale z_0^T (where T stands for "thermal") and from (3) and (4) we get

$$w'_0 \sim (Qz_0^T)^{\frac{1}{3}} \tag{5}$$

and

$$B'_0 \sim Q^{\frac{2}{3}} z_0^{T\,-\frac{1}{3}} \,. \tag{6}$$

Similar to the buoyancy perturbations, the mean buoyancy above the roughness scale has to vary as $z^{-\frac{1}{3}}$. We thus find

$$\bar{B} - \bar{B}_0 \sim Q^{\frac{2}{3}} [(z_0^T)^{-\frac{1}{3}} - z^{-\frac{1}{3}}] \,. \tag{7}$$

This result implies that for $z \gg z_0^T$, $\bar{B}$ converges to the constant value $\bar{B} \sim Q^{\frac{2}{3}} z_0^{T\,-\frac{1}{3}}$ which is determined by the surface flux and the roughness length.

Note that the above arguments change dramatically if an upper lid would be considered. In this case another length scale h given by the height of the domain would exist. The turbulent velocity scale in this case is given by the Deardorff [2] scaling.

$$w' \sim (Qh)^{\frac{1}{3}} \tag{8}$$

If more than one length scale exists in the problem, simple scaling laws can generally no longer be found, since all quantities can be functions of the non-dimensional numbers that are then intrinsic to the problem.

1.2 Shear Driven Boundary Layers

A similar analysis can be performed if turbulence is dominated by mechanical forcing. Again assuming a semi-infinite domain we find that the flux of momentum through the boundary is given by

$$M = \int_0^\infty (\dot{u}) dz \tag{9}$$

where $\dot{u}$ generally represents any velocity source. In a steady state and in a nonrotating system (or if rotation can be neglected on the regarded scales) we find:

$$M = \int_0^\infty \frac{1}{\rho} \frac{\partial p}{\partial x} dz \,. \tag{10}$$

M has the dimension of a velocity squared. Defining $u^{*2} \equiv M$ we directly find that the turbulent velocity has to scale as

$$w' \sim u^* \tag{11}$$

and is thus constant with height, unlike in the buoyancy driven case. A scaling for the shear of the mean wind is given by

$$\frac{d\bar{u}}{dz} \sim \frac{u^*}{z} \,. \tag{12}$$

Integrating and assuming that $\bar{u}$ vanishes at z_0, which is the roughness length for momentum, gives

$$\bar{u} \sim u^* \ln \frac{z}{z_0} \,. \tag{13}$$

And for the background velocity difference between the heights z_1 and z_2

$$\Delta\bar{u} \sim u^* \ln \frac{z_2}{z_1} \,. \tag{14}$$

This can be solved to get an equation for the surface momentum flux

$$M = u^{*2} \sim \frac{(\Delta\bar{u})^2}{(\ln \frac{z_2}{z_1})^2} \,. \tag{15}$$

This equation allows one to determine the surface flux from a given mean velocity profile (given that the necessary proportionality constant is determined).

More generally, scaling analysis show that the surface flux of any tracer θ in a mechanically driven boundary layer is given by

$$F = cu^*(\bar{\theta}_0 - \bar{\theta}_a) \,, \tag{16}$$

where $\bar{\theta}_a$ denotes the background tracer concentration at some fixed height and c is a constant that depends on the choice of this height. For more details on the derivation of this equation see chapter three in [4].

1.3 Boundary Layers with Shear and Convection

In real atmospheric boundary layers, thermal convection and vertical shear of the background flow usually come together. Assuming prescribed surface fluxes of buoyancy and momentum, Q and M, a natural length scale is given by

$$L = \frac{M^{\frac{3}{2}}}{Q_0} = \frac{u^{*3}}{\overline{w'B'}}\,. \tag{17}$$

This is referred to as the Monin-Obukov length[1]. It can be gained by comparing the turbulent vertical velocities in the buoyancy driven boundary layer (3) and in the shear driven boundary layer (11). This makes clear that the Monin Obukov length separates the boundary into regions where the turbulence is dominantly driven by shear ($z \ll L$) and by convection ($z \gg L$). Since this adds a lengthscale to the system, all vertical dependences of quantities can now contain functions of the nondimensional number z/L, which can obviously not be determined from simple scaling laws.

1.4 The Linear WISHE Model

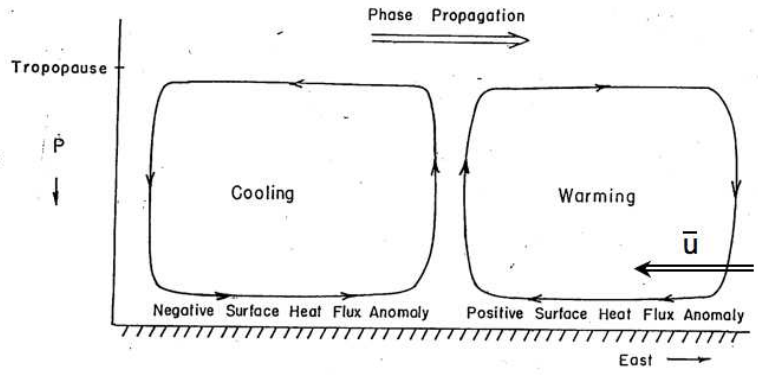

Figure 2: Sketch of the mechanism acting in the WISHE model. Positive superposition of the background easterlies with the easterly disturbance gives rise to an increased surface buoyancy flux, while the partial cancellation of the background flow and the disturbance reduces the buoyancy flux on the left.

The fact that when a momentum source is present, the surface flux of heat depends on the surface wind speed can cause a convective disturbance in the presence of a background flow to grow and propagate, as sketched in figure 2. A simple linear model describing this will be derived in this section. The model is a dry version of the WISHE model derived in [3]. Assuming that the surface heat flux is dominated by mechanically driven turbulence, we can use equation (16) to get the buoyancy flux at the surface

$$Q = c_2 u(B_s - B)\,, \tag{18}$$

[1]Strictly speaking the Monin-Obukov length is conventionally defined with the opposite sign, thus being negative if the surface buoyancy flux is positive

where B_s denotes the buoyancy at the surface (which will be assumed to be constant in the following) while B denotes the buoyancy at some fixed finite height above the surface. All variables in (18) denote mean values over a temporal and spatial scale larger than the scale of the background turbulence. In the following we will consider two-dimensional pertubations u', B' with much larger temporal and spatial scale then the background turbulence and a constant zonal background flow $\bar{u}$ and buoyancy $\bar{B}$. We further assume that the buoyancy fluctuations are constant with height over the whole depth h of the boundary layer[2]. This is generally a good approximation in a convective layer. Linearizing in the perturbations we then get for the anomalous surface heat flux

$$Q' = h\left(\frac{\partial B'}{\partial t} + \bar{u}\frac{\partial B'}{\partial x}\right) = [c_2 u'(B_s - \bar{B}) - c_2 \bar{u} B']|_{z=0}\,, \tag{19}$$

where h is the depth of the boundary layer.

The vorticity equation in the x-z plane becomes

$$\left(\frac{\partial}{\partial t} + \bar{u}\frac{\partial}{\partial x}\right)\Delta\psi = \frac{\partial B'}{\partial x} \tag{20}$$

where we used the incompressibility condition which allows us to introduce a streamfunction so that

$$u' = -\frac{\partial \psi}{\partial z} \qquad \text{and} \quad w' = \frac{\partial \psi}{\partial x}\,. \tag{21}$$

Rescaling

$$(x, z) \to h(x, z) \qquad \text{and} \quad t \to \frac{h}{\bar{u}} t \tag{22}$$

and using (19) and (21), we get

$$\left(\frac{\partial}{\partial t} + \frac{\partial}{\partial x}\right)^2 \Delta\psi = -\left[\alpha \frac{\partial^2 \psi}{\partial x \partial z} + c_2\left(\frac{\partial}{\partial t} + \frac{\partial}{\partial x}\right)\Delta\psi\right]_{z=0} \tag{23}$$

where

$$\alpha = \frac{\bar{Q} h}{\bar{u}^3}\,.$$

Using an approach of the form $\psi = f(y)\exp(i(kx - ct))$ this can be solved for the phase velocity $c_r = \Re(c)$ and growth rate $\sigma = \Im(c)$. The results for $c_2 = 10^{-3}$ and $\alpha = 1$ as well as $\alpha = 5$ are shown in figure 3. We find exponentially growing disturbances in all cases. The growth rate increases with wavenumber, though the increase stagnates as the wavelength becomes short compared to the depth of the fluid. Further we find that the phase velocity relative to the mean flow is always opposite to the latter. For large α, i.e. small background flows or strong heatflux, and long horizontal wavelength, we even find absolute phase propagation opposite to the mean flow.

[2]The boundary layer here is in general the convective part of the atmosphere up to the first inversion. In the tropics this would usually be the tropopause

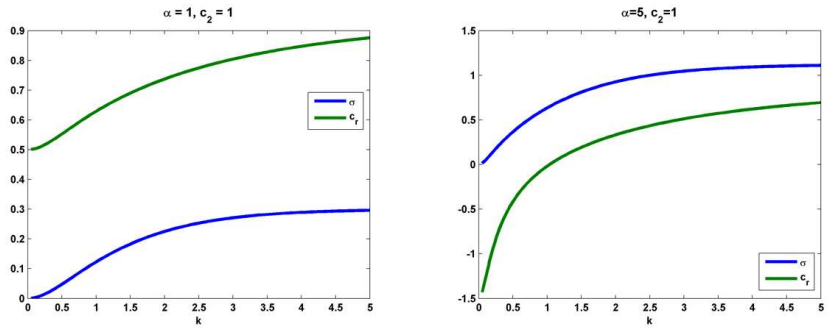

Figure 3: Left: Nondimensional growth rate (blue) and phase propagation (green) for the WISHE model with $\alpha = 1$ and $c_2 = 10^{-3}$. Right: As left but for $\alpha = 5$. Note that the mean flow has velocity 1, i.e. the phase propagation relative to the mean flow is always negative.

1.5 Radiative Equilibrium and Thermodynamic Disequilibrium

Convective adjustment is an important process in the atmosphere, because radiative equilibrium temperature profiles are generally in thermodynamic disequilibrium with the surface. This shall be illustrated here with a simple layered radiative equilibrium model for the atmosphere.

The model is sketched in figure 4. The incoming shortwave radiation is described by an equivalent effective emission temperature T_e. The atmosphere consists of one layer which is completely opaque ($\epsilon = 1$) for longwave radiation but transparent to short-wave radiation.An additional thin layer ($\epsilon_A \ll 1$) represents the atmospheric boundary just above the surface. The radiative equilibrium for the whole system directly yields that

$$T_1 = T_e \,. \tag{24}$$

From the radiative equilibrium for the surface and the boundary layer, and neglecting the radiative effects of this thin surface layer, layer we find

$$T_s{}^4 = T_e{}^4 + T_1{}^4 \tag{25}$$

and

$$2T_A{}^4 = T_1{}^4 + T_s{}^4 \,. \tag{26}$$

This yields

$$T_A{}^4 = \left(\frac{3}{4}\right) T_s{}^4 \tag{27}$$

and therefore $T_A < T_s$. We thus find that in radiative equilibrium the temperature of the atmosphere right above the surface would be lower than the surface temperature itself which would be instable and trigger convection. Qualitatively similar result are obtained with more complex continuous radiative equilibrium models. Thus radiative equilibrium states will generally have convecting boundary layers.

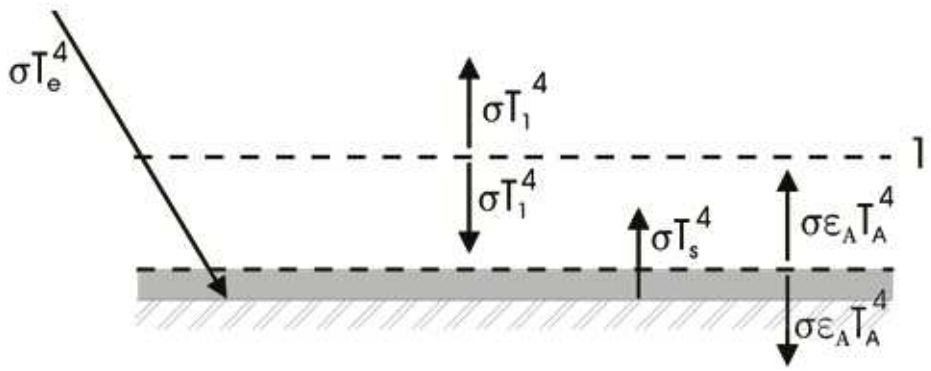

Figure 4: Sketch of a radiative equilibrium model. See text for details.

2 Compressible Convection

For a homogeneous fluid, the specific volume α (=$1/\rho$) can be expressed as a function of two variables, which are chosen to be pressure p and entropy s_d here, i.e. $\alpha = \alpha(p, s_d)$. The entropy (in dry case) s_d is defined by:

$$s_d = c_p \ln(\frac{T}{T_o}) - R_d \ln(\frac{p}{p_o}) \tag{28}$$

where T_o and p_o are reference temperature and pressure. We can derive buoyancy B based on entropy s_d:

$$\begin{aligned} B &= -g\frac{(\delta\rho)_p}{\rho} && (29) \\ &= g\frac{(\delta\alpha)_p}{\alpha} \\ &= -\frac{dp}{dz}(\delta\alpha)_p \quad \text{(by hydrostatic balance)} && (30) \end{aligned}$$

then, since

$$(\delta\alpha)_p = (\frac{\partial\alpha}{\partial s_d})_p \delta s_d = (\frac{\partial T}{\partial p})_{s_d} \delta s_d, \tag{31}$$

where the last equation is because of the Maxwell equation:

$$(\frac{\partial\alpha}{\partial s_d})_p = (\frac{\partial T}{\partial p})_{s_d} \tag{32}$$

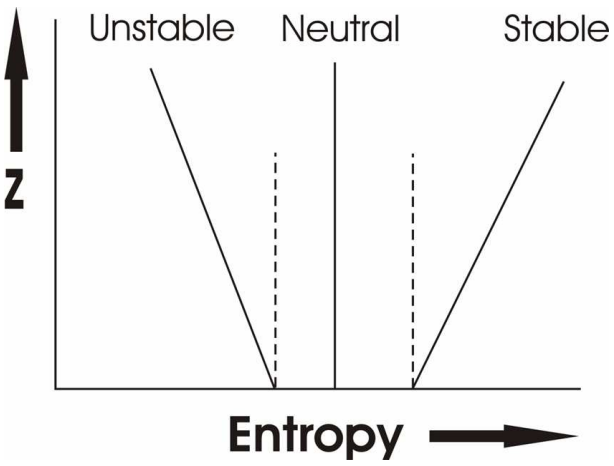

Figure 5: Entropy s_d as a function of height z.

$$\begin{aligned} B &= -\frac{dp}{dz}(\frac{\partial T}{\partial p})_{s_d}\delta s_d \quad \text{(plug equation 31 into 30)} \\ &= -(\frac{\partial T}{\partial z})_{s_d}\delta s_d \qquad (33) \\ &\equiv \Gamma \delta s_d \qquad (34) \end{aligned}$$

where $\Gamma \equiv -(\frac{\partial T}{\partial z})_{s_d}$ = dry adiabatic lapse rate (rate of change of T for a parcel of air moved vertically and adiabatically) $= \frac{g}{c_p} = 9.8K/km$ for the Earth's atmosphere.

The potential temperature θ, a measure of the entropy of a gas, is defined by

$$\theta = T(\frac{p_o}{p})^{R/c_p} \qquad (35)$$

where p is the pressure, p_o some reference pressure, R the ideal gas constant, and c_p the heat capacity of the gas at constant pressure. The relation between θ and s_d is given by:

$$s_d = c_p \ln(\theta) + constant. \qquad (36)$$

Both variables are conserved for reversible dry adiabatic processes. Figure 5 shows the stability of entropy as a function of height. It is unstable if entropy decreases with height while it is stable if entropy increases with height. A model aircraft measurement in a desert region near Albuquerque, New Mexico, on August 1993 is shown in Figure 6. In this dry case, the virtual potential temperature doesn't change much with height and the mean entropy is conserved [7].

However, above a thin boundary layer, most atmospheric convection involves phase change of water. Moist convection has significant heating owing to phase changes of water, and helps global redistribution of water vapor. Water vapor, being one of the most important greenhouse gases, is the primary tropospheric infrared absorber while condensed phases are a significant contributor to stratiform cloudiness which absorb infrared radiation and scatter short wave radiation as well. Figure 7 shows the phase equilibria of H_2O, and changes of phase cause significant release or absorption of heat.

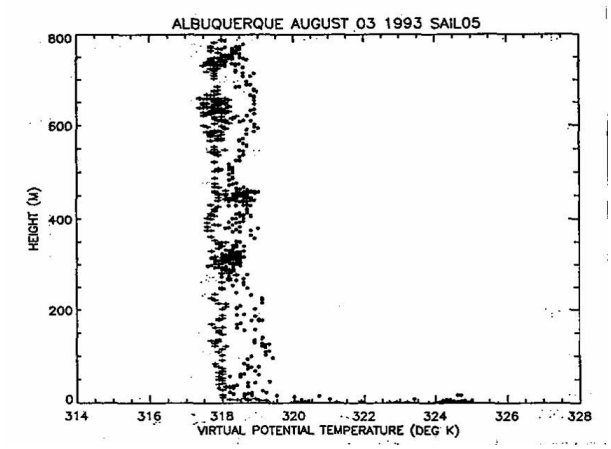

Figure 6: Observations of virtual potential temperature made with an RPV (remotely piloted vehicle) flight in a desert region near Albuquerque, New Mexico, on August 1993. The observations during ascent (inside the plume) are represented by dots; observations on descent (outside of the plume) are represented by crosses.

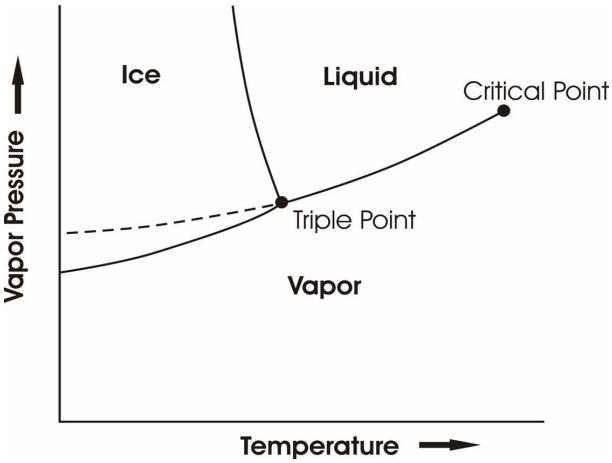

Figure 7: Phase equilibria of H_2O.

The equation of state for water vapor is given by:

$$e\alpha_v = R_v T \tag{37}$$

where e is the vapor pressure, α_v the specific volume for water vapor, and $R_v = R\frac{\overline{m}}{m_v}$ the gas constant for water vapor.

$$e = \frac{R_v T}{\alpha_v} = \frac{R\frac{\overline{m}}{m_v}T}{\alpha_v} = qp\frac{\overline{m}}{m_v} \tag{38}$$

gives the expression for vapor pressure, where q is the mass concentration of water vapor, $\overline{m}$ the mean molecular weight of air, m_v the molecular weight for water vapor. Saturation vapor pressure e^* is also a function of T, i.e. $e^* = e^*(T)$. If we decrease p(or q), both e and e^* will decrease, but since e^* decreases more rapidly, i.e. $e > e^*$, water vapor will be supersaturated.

Supersaturated vapor always condenses onto ambient aerosols called cloud condensation nuclei in a process called heterogeneous nucleation. Cloud condensation nuclei include sea salt from bursting bubbles, windblown dust, combustion products (i.e., organic carbon and soot), photochemically-produced sulfate (i.e., smog), volcanic aerosols, and meteoric debris. The drop size distribution is quite sensitive to the size distribution of cloud condensation nuclei. While stochastic coalescence is a way to form precipitation, the Bergeron-Findeisen process is another important alternative way of initiating precipitation in mid-latitude clouds. Precipitation formation is a strongly nonlinear function of the cloud water concentration. The time scale of precipitation formation is about 10 to 30 minutes.

We used entropy s_d to discuss the stability for dry air, and specific volume α can be expressed as a function of s_d and p, i.e. $\alpha = \alpha(s_d, p)$. In the moist convection case, we can define an approximately conserved thermodynamic variable, the specific entropy s, a function of temperature, pressure, and water concentration,

$$s = c_p \ln(\frac{T}{T_o}) - R_d \ln(\frac{p}{p_o}) + L_v\frac{q}{T} - qR_v \ln(H) \tag{39}$$

where $H \equiv \frac{e}{e^*}$ = relative humidity. Specific volume α now depends on three variables rather than two, i.e. $\alpha = \alpha(s, p, q_t)$, where q_t is the total concentration of H_2O of all phases, thus we cannot compare the densities of two samples at the same pressure using just a single entropy variable, a fact of profound consequences for the character of moist convection. But we can make progress by first defining a saturation entropy s^*, the specific entropy air would have if it were saturated with water vapor at the same temperature and pressure. It is given by:

$$s^* = c_p \ln(\frac{T}{T_o}) - R_d \ln(\frac{p}{p_o}) + \frac{L_v q^*}{T} = s(T, p, q^*) \tag{40}$$

and

$$\alpha = \alpha(s^*, p, q_t) \tag{41}$$

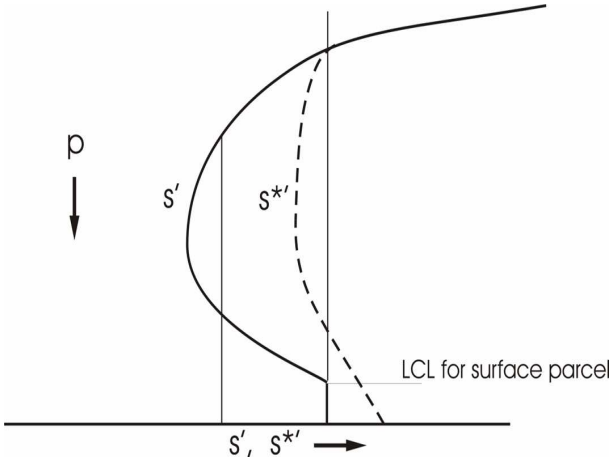

Figure 8: Structure of s' and $s^{*\prime}$.

Then we can add an arbitrary function of q_t to s^* such that the specific volume can be expressed approximately by two variables,

$$\alpha \cong \alpha(s^{*\prime}, p) \tag{42}$$

Figure 8 gives the profile of entropy s' and saturation entropy $s^{*\prime}$ of the surrounding atmosphere. The straight upward lines are the entropy profile of a parcel which is lifted upward or downward since entropy is conserved. If a parcel is lifted upward with the same entropy as the surrounding atmosphere at the surface, it will rise dry adiabatically until reaching the lifting condensation level (LCL); further ascent will be saturated adiabatic. However only until reaching the crossing point with $s^{*\prime}$ will the parcel be stable; after that the parcel would attain positive buoyancy since its entropy (which will equal its saturation entropy since by then the parcel is saturated) will be larger than that of its environment.

Tropical temperature soundings are, to a first approximation, moist adiabatic. Figure 9 is a buoyancy diagram, showing the difference between the density temperature (a temperature that has been corrected for the presence of water vapor and condensed water, so as to accurately measure the density of the air sample) of a reversibly lifted parcel and that of its environment, as a function of the level from which the parcel is lifted and the level to which it is lifted. Note that the environment is almost neutral to a parcel lifted reversibly from around 950 hPa.

When condensed water precipitates, this irreversible process depletes water from the ascending cloudy currents and causes much of the air to be subsaturated when it subsequently descends. Updrafts due to convective instability can be quite strong over a very small fractional area. After reaching the level of neutral buoyancy, it diverges and spreads out laterally, injecting its properties into the large-scale environment. In equilibrium, the surface enthalpy flux F_k, which is given by $C_k\rho|V|(k_o^* - k_a)$, with k_o^* representing the saturation enthalpy of air in contact with the ocean and k_a the enthalpy at the boundary, should be equal to the vertically integrated radiative cooling, where C_k is the enthalpy exchange coefficient, $|V|$ the magnitude of the surface wind, and the specific enthalpy k given by $k = c_pT + L_vq$.

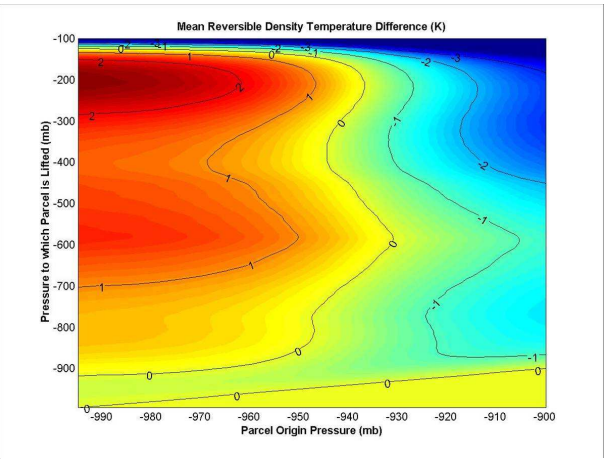

Figure 9: Contour plot of the difference between the environmental density temperature and the density temperature of a parcel lifted reversibly and adiabatically from the pressure level given on the abscissa to the pressure level on the ordinate. This quantity has been averaged over several thousand soundings taken at Kapingamarangi in the tropical western South Pacific.

3 Hurricanes and friends

There are lots of meteorological phenomena related to waves and vortices driven by interfacial fluxes, such as hurricanes, polar lows, dust devils, agukabams, and convectively coupled equatorial waves.

Figure 10 shows the equivalent potential temperature (a measure of moist entropy)of Hurricane Inez in September 28, 1966 as a function of radial distance from the geometrical center of the eye and pressure. Note that the entropy is high at the hurricane center.

By using conserved variables, such as energy, saturation entropy and angular momentum, the potential intensity of the hurricane within the eyewall region can be expressed as:

$$|V|^2 = \frac{C_k}{C_D}\frac{T_s - T_o}{T_o}(k_o^* - k) \tag{43}$$

where C_D is the surface drag coefficient, T_s the sea surface temperature and T_o the temperature at the top of the hurricane [1].

Like the engine in a Carnot Cycle, the energy cycle of hurricanes is one of isothermal expansion, adiabatic expansion, isothermal compression and adiabatic compression. The total rate of heat input to the hurricane is given by:

$$\dot{Q} = 2\pi \int_0^{r_o} \rho[C_k|V|(k_o^* - k) + C_D|V|^3]rdr \tag{44}$$

where r_o is the radius from the storm center, and the first term within the square brackets is the surface enthalpy flux and the second one is the dissipative heating. In steady state, work is used to balance frictional dissipation:

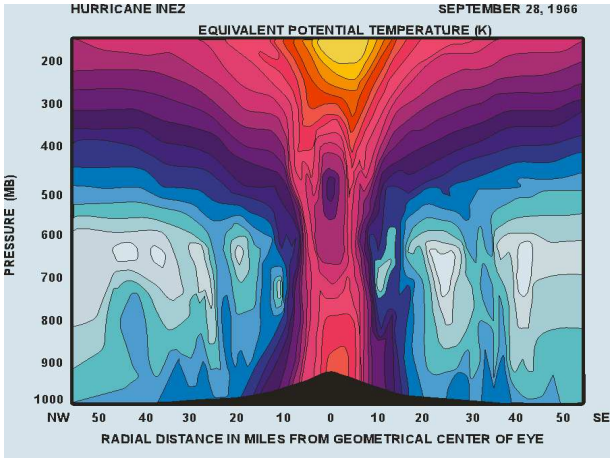

Figure 10: Equivalent potential temperature of Hurricane INEZ in September 28, 1966 as a function of radial distance from the geometrical center of the eye and pressure.

$$W = 2\pi \int_0^{r_o} \rho[C_D|V|^3]rdr \tag{45}$$

$$= \frac{T_s - T_o}{T_s}\dot{Q} \tag{46}$$

$$= 2\pi \frac{T_s - T_o}{T_s} \int_0^{r_o} \rho[C_k|V|(k_o^* - k) + C_D|V|^3]rdr. \tag{47}$$

If we assume that the integrals are dominated by the values of their integrands near the radius of maximum wind speed, then it gives an approximate expression for the maximum wind speed:

$$|V_{max}|^2 \cong \frac{C_k}{C_D}\frac{T_s - T_o}{T_o}(k_o^* - k) \quad [6]. \tag{48}$$

This equation, however, can be derived exactly from considerations of thermal wind balance. Figure 11 shows the maximum wind speed profile as a function of sea surface temperature (SST) and T_o when the relative humidity is 0.75 and C_k/C_D equals 1.2.

Figures 12 and 13 exhibit the relationship between the potential intensity (PI) and intensity of real tropical cyclones [5] [6]. Since the cumulative distribution function (CDF) is linear for tropical storms, within each regime, there is a roughly equal likelihood of a given storm reaching any given intensity up to its potential intensity. In addition, CDFs of the wind speeds in North Atlantic and western North Pacific tropical cyclones were calculated. The peak winds reached during the storms, normalized by their theoretical maximum values, tend to fall into one of two linear CDFs depending on whether the storm does or does not reach hurricane intensity, as shown in Figure 9. This means that a randomly chosen tropical cyclone has the same probability of reaching any given intensity up to marginal hurricane intensity, and another probability of reaching any intensity between marginal hurricane intensity and the maximum theoretical intensity at that time and place.

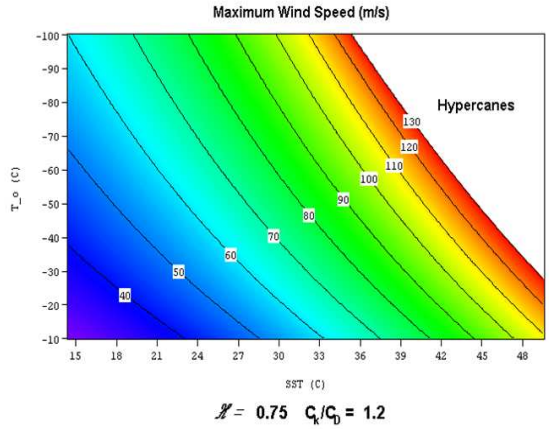

Figure 11: Maximum wind speed profile as a function of sea surface temperature (SST) and T_o when the relative humidity is 0.75 and C_k/C_D equals 1.2.

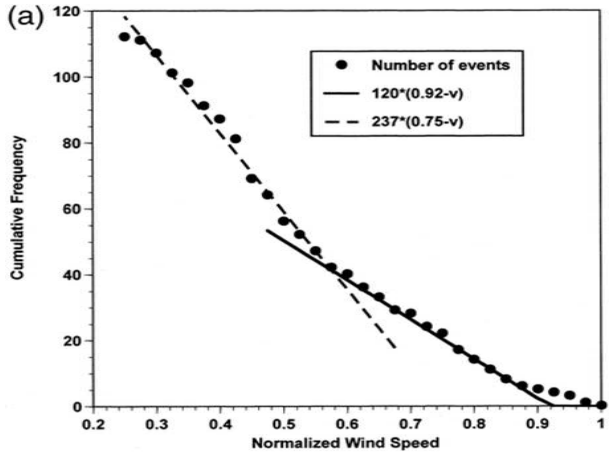

Figure 12: Cumulative distribution function (CDF) of lifetime maximum wind speeds for all tropical cyclones of tropical storm strength 18 m s^{-1} or greater after 1957 whose lifetime maximum intensity was not limited by declining potential intensity. Wind speed is normalized by monthly climatological potential wind speed at the reported position of the tropical cyclones. The ordinate shows the total number of events whose normalized lifetime maximum wind speed exceeds the value on the abscissa.

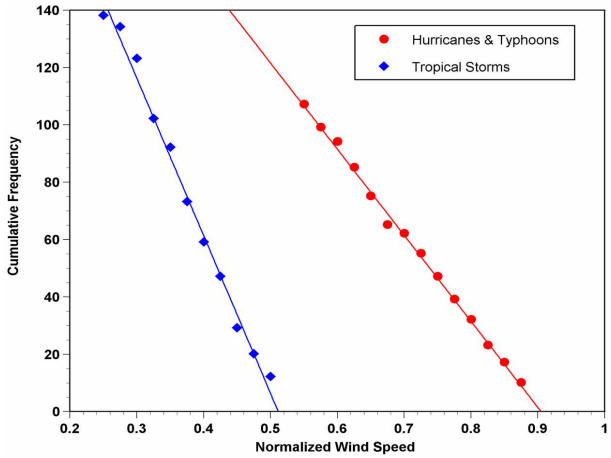

Figure 13: Total number of tropical cyclones with normalized wind speeds exceeding the value on the abscissa, from 1957 to 1999 in the North Atlantic and from 1970 to 1999 in the western North Pacific. Wind speed is normalized by the theoretical maximum wind speed calculated from climatological data.

Polar lows, agukabams, dust devils and convectively coupled equatorial waves are, together with hurricanes, meteorological phenomena related to waves and vortices driven by interfacial fluxes. Polar lows have similar mechanisms as hurricanes, but they are small-scale storms with ice. Their smaller scale is consistent with theoretical estimates of the maximum radius of a convective storm which is proportional to $1/f$. Agukabams draw their energy from enthalpy transferred from hot, moist soils. When agukabams happen, there is usually a big drop in the soil temperature, reflecting the heat transferred from the soil to the air. Dust devils are essentially dry hurricanes, and like agukabams, they draw energy from the sensible heat of the sand. It has been observed that Dust devils happen not only on the Earth but also on Mars.

For convectively coupled equatorial waves, a wavenumber-frequency spectrum analysis of the satellite-observed outgoing longwave radiation (OLR) was performed within the region between $15^oS - 15^oN$ by Wheeler and Kiladis (1999) [8]. After removing an estimated background spectrum, the spectral peaks correspond nicely with dispersion relations from equatorially trapped wave modes of shallow water theory. Figure 14 shows the symmetric component of OLR and some peaks corresponding to the dispersion relations of the equatorially trapped wave modes. These so-called convectively coupled equatorial waves are the Kelvin, $n = 1$ equatorial Rossby wave, mixed Rossby-gravity, $n = 0$ eastward inertio-gravity, $n = 1$ westward inertio-gravity (WIG), and $n = 2$ WIG waves. The Madden-Julian oscillation (MJO) and the tropical depression-type (TD-type) disturbances are also present in the spectra, but they are unlike the convectively coupled equatorial waves due to their location away from the equatorial wave dispersion curves in the wavenumber-frequency spectrum.

References

[1] M. Bister and K. A. Emanuel, *Dissipative heating and hurricane intensity.*, Mete-

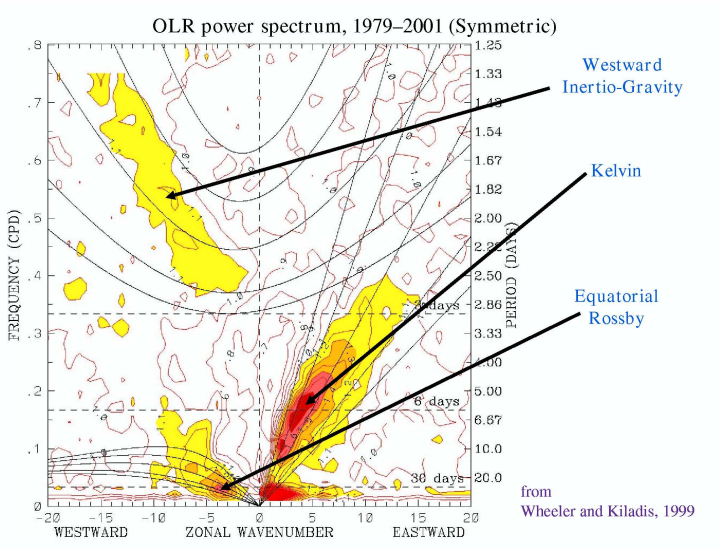

Figure 14: Symmetric components of the OLR. The spectral peaks correspond quite well to the dispersion relations of the equatorially trapped wave modes.

orol. Atmos. Phys., 65 (1998), pp. 233–240.

[2] J. W. Deardorff, *Convective velocity and temperature scales for the unstable planetary boundary layer and for rayleigh convection*, J. Atmos. Sci., 27 (1970), pp. 1211–1213.

[3] K. A. Emanuel, *An air-sea interaction model of intraseasonal oscillations in the tropics*, J. Atmos. Sci., 44 (1987), pp. 2324–2340.

[4] ——, *Atmospheric Convection*, Oxford University Press US, 1994.

[5] ——, *A statistical analysis of hurricane intensity.*, Mon. Wea. Rev., 128 (2000), pp. 1139–1152.

[6] ——, *Tropical cyclones*, Annu. Rev. Earth Planet Sci., 31 (2000), pp. 75–104.

[7] N. O. Rennó and E. R. Williams, *Quasi-lagrangian measurements in convective boundary layer plumes and their implications for the calculation of cape.*, Mon. Wea. Rev., 123 (1995), pp. 2733–2742.

[8] M. Wheeler and G. N. Kiladis, *Convectively coupled equatorial waves: Analysis of clouds and temperature in the wavenumbercfrequency domain.*, J. Atmos. Sci., 56 (1999), pp. 374–399.